

A Latent Factor Panel Approach to Spatiotemporal Causal Inference

Jiaxi Wu
UCSB

Alexander Franks
UCSB

September 16, 2025

Abstract

Unmeasured confounding can severely bias causal effect estimates from spatiotemporal observational data, especially when the confounders do not vary smoothly in time and space. In this work, we develop a method for addressing unmeasured confounding in spatiotemporal contexts by building on models from the panel data literature and methods in multivariate causal inference. Our method is based on a *factor confounding* assumption, which posits that effects of unmeasured confounders on exposures and outcomes can be captured by a shared latent factor model. Factor confounding is sufficient to partially identify causal effects, even when there is interference between units. Additional assumptions that limit the degree of spatiotemporal interference, reasonable in most applications, are sufficient to point identify the effects. Simulation studies demonstrate that the proposed approach can substantially reduce omitted variable bias relative to other spatial smoothing and panel data baselines. We illustrate our method in a case study of the effect of prenatal PM_{2.5} exposure on birth weight in California.

Keywords: Causal inference; environmental health; factor models; panel data; spatiotemporal data; unmeasured confounding.

1 Introduction

Causal inference with spatial data is essential in disciplines where exposures are determined by geography rather than experimental design—for instance, environmental exposures in epidemiology (Bind, 2019) and neighborhood socioeconomic conditions in public health research (Diez Roux, 2001). In such contexts, researchers cannot randomize who is exposed to polluted air, which census tract receives a policy intervention, or which areas are prioritized for infrastructure development. Instead, they must draw causal insights from observational data in which sampling units are embedded in space. The spatial configuration presents both opportunities—through natural variation and spatial dependence—and challenges, as exposures, covariates, and outcomes often co-vary spatially. However, as in any observational study, the validity of causal conclusions hinges on untestable assumptions about the confounding mechanism. The term *spatial confounding* has been used to describe a number of phenomena arising from either the data generation process or the analysis model (Hodges and Reich, 2010; Khan and Berrett, 2023). Following the causal perspective of Gilbert et al. (2021), we focus on unmeasured confounders that simultaneously influence both the exposure and the outcome.

Recent work in spatial statistics has examined the conditions under which different spatial and causal methods account for spatial confounding (Reich et al., 2021). For example, Thaden and Kneib (2018) and Dupont et al. (2022) employ two-stage procedures to partial out spatial confounding. Papadogeorgou et al. (2019) incorporate spatial proximity into propensity score matching to adjust for unmeasured confounding, while Schnell and Papadogeorgou (2020) model the joint distribution of the exposure and unmeasured confounders parametrically to mitigate bias. Papadogeorgou and Samanta (2023) propose a Bayesian parametric approach to account for entangled spatial confounding and interference. Most existing approaches depend on parametric assumptions regarding the relationships between unobserved confounders and observed variables, often focusing on specific estimands or analysis frameworks. In contrast, Gilbert et al. (2021) formalize a set of nonparametric identification assumptions for geostatistical (point-referenced) data, requiring the unmeasured confounder to be a fixed, measurable function of spatial location.

A common premise behind many adjustments for spatial confounding is that the exposure varies at a finer spatial scale than the spatial confounder (Paciorek, 2010; Keller and Szpiro, 2020; Guan et al., 2023), or exhibits sufficient non-spatial variation to satisfy the positivity assumption required for causal identification (Bobb et al., 2022; Schnell and Papadogeorgou, 2020; Gilbert et al., 2021). Scale-separation approaches operationalize this premise by decomposing spatial signals into frequency bands and filtering low-frequency confounding. In settings with multiple exposures and outcomes, Prim et al. (2025) develop a spectral-domain adjustment by projecting to scale-specific components under a local unconfoundedness condition. In practice, however, unmeasured confounders may vary over space, fluctuate over time, and display idiosyncratic differences across units, leading to mixed spatial and non-spatial structure. Such complexity limits the effectiveness of existing methods that rely solely on spatial (or spatiotemporal) smoothing to adjust for confounding bias.

To account for some of these complexities, we leverage ideas from the panel data literature. Causal panel methods are designed to handle unobserved heterogeneity across multiple units measured repeatedly, most commonly applied to settings with binary exposures and

well-defined pre- and post-treatment periods. Popular approaches include classical two-way fixed effects, difference-in-differences, and synthetic control or factor-based methods (see e.g. Ben-Michael et al., 2021; Arkhangelsky and Imbens, 2024, for a review). Of particular relevance is the interactive fixed effects (IFE) model of Bai (2009), which represents unobserved heterogeneity through a low-rank decomposition of time-varying latent factors and unit-specific loadings. This method accommodates continuous exposures and yields asymptotically consistent estimates under linear outcome models, provided that both the cross-sectional and temporal dimensions are sufficiently large.

Our approach also builds on recent advances in causal inference with multiple exposures (Miao et al., 2022; Zheng et al., 2025) and multiple outcomes (Zheng et al., 2024; Kang et al., 2025). With appropriate assumptions, causal effects can be partially identified, underscoring the importance of linking identification assumptions to causal conclusions in a transparent and interpretable manner (Zheng et al., 2022). One common strategy leverages shared confounding via the use of proxy variables or negative controls to identify causal effects or detect bias (Shi et al., 2020; Tchetgen Tchetgen et al., 2024). These methods rely on variables that are assumed to be associated with the unmeasured confounder but are known not to directly influence the outcome (negative control exposures) or not to be affected by the exposure (negative control outcomes). While negative controls have been explored in the context of time-series and longitudinal studies, their application to spatial settings remains limited, with some exceptions (e.g. Lumley and Sheppard, 2000).

1.1 Contribution

In this work, we develop a flexible framework for reasoning about causal effects in spatiotemporal settings with unmeasured confounding and potential interference. Gilbert et al. (2021) show that it is possible to identify causal effects from spatial data as long as unmeasured confounders are a deterministic measurable function of the spatial location. However, even when such assumptions hold in principle, reliable estimation can fail in practice when the number of sampled sites is small or in applications with short-range correlations or non-stationarity. In order to handle such situations, we apply recent results related to multivariate causal inference with latent variables to account for residual spatiotemporal variation. Previous studies have shown that when there are multiple measurements on a unit sharing a common confounding mechanism, latent variable models can facilitate (partial) identification by leveraging the shared information—typically across multiple exposures or outcomes within each unit (Zheng et al., 2024, 2025; Kang et al., 2025). We extend this idea of exploiting *within-unit* associations to modeling *between-unit* dependencies, where latent confounders induce correlations across space and/or time points.

We show that when exposures and outcomes are linear in the unmeasured confounders, with appropriate conditions, factor models can facilitate partial identification of causal effects. We then establish precise limits on the degree of spatiotemporal interference that can be incorporated while maintaining causal identification. In addition, our approach is compatible with a wide range of models, including those that allow for treatment effect heterogeneity. We provide theoretical guarantees, conduct extensive simulations benchmarking our approach against commonly used methods, and demonstrate its practical utility through a case study estimating the effect of $PM_{2.5}$ exposure on birth weight in California.

2 Problem Setup

Let $\mathcal{I} = \{1, \dots, N\}$ index spatial locations and $\mathcal{T} = \{1, \dots, T\}$ index time points. For each location-time pair $(i, t) \in \mathcal{I} \times \mathcal{T}$, we observe $(D_{it}, Y_{it}, \mathbf{X}_{it}, \mathbf{S}_i)$ drawn from a joint spatiotemporal data generating process \mathcal{P} , where $D_{it} \in \mathbb{R}$ is the exposure (or treatment), $Y_{it} \in \mathbb{R}$ is the outcome, $\mathbf{X}_{it} \in \mathbb{R}^p$ is a vector of observed pre-exposure covariates, and $\mathbf{S}_i \in \mathbb{R}^{p_s}$ denotes the spatial coordinates of location i (e.g., $p_s = 2$ for longitude and latitude). Collect the exposures and outcomes into $\mathbf{D} = (D_{it}) \in \mathbb{R}^{N \times T}$ and $\mathbf{Y} = (Y_{it}) \in \mathbb{R}^{N \times T}$, with \mathbf{D}_t and \mathbf{Y}_t denoting the N -vectors at time t , and \mathbf{D}_i and \mathbf{Y}_i denoting the T -vectors at location i .

Let $Y_{it}(\mathbf{d})$ be the potential outcome that would have been observed at (i, t) had all exposures been set to \mathbf{d} (Rubin, 1974). The dimensionality of potential outcomes can be reduced under the partial interference assumption (Reich et al., 2021; Papadogeorgou and Samanta, 2023). Specifically, we assume that for each (i, t) , Y_{it} depends only on exposures in the neighborhood $\mathcal{N}_{it} \subseteq \mathcal{I} \times \mathcal{T}$:

Assumption 1 (Partial interference). *For every (i, t) and exposure \mathbf{d} , $Y_{it}(\mathbf{d}) = Y_{it}(\mathbf{d}_{\mathcal{N}_{it}})$, where $\mathbf{d}_{\mathcal{N}_{it}} := \{d_{jk} : (j, k) \in \mathcal{N}_{it}\} \in \mathbb{R}^{|\mathcal{N}_{it}|}$.*

Common choices include: no interference, where $\mathcal{N}_{it} = \{(i, t)\}$; spatial neighbors, where $\mathcal{N}_{it} = \{(j, t) : j \in \mathcal{I}\}$; or temporal interference such that $\mathcal{N}_{it} = \{(i, k) : k \leq t\}$. It is common to further summarize the exposure through a measurable map $\mathbf{A}_{it} = f_{it}(\mathbf{D}_{\mathcal{N}_{it}})$, for instance $\mathbf{A}_{it} = (D_{it}, \bar{D}_{it})$ with \bar{D}_{it} the neighborhood mean (Aronow and Samii, 2017). The potential outcome can be written as $Y_{it}(\mathbf{d}) = Y_{it}(\mathbf{d}_{\mathcal{N}_{it}}) = Y_{it}(\mathbf{a})$. The population average treatment effect (PATE) comparing two interventions $\mathbf{d}^{(1)}$ and $\mathbf{d}^{(2)}$ is defined as

$$\text{PATE}(\mathbf{d}^{(1)}, \mathbf{d}^{(2)}) := \mathbb{E} \left[Y_{it}(\mathbf{d}_{\mathcal{N}_{it}}^{(1)}) - Y_{it}(\mathbf{d}_{\mathcal{N}_{it}}^{(2)}) \right],$$

where the expectation is taken over the population distribution \mathcal{P} . This estimand includes, as special cases, the direct effect, where the two exposure vectors differ only in the exposure of the index unit (i, t) , with all neighbors' exposures held fixed, and the indirect (interference) effect, where they differ only in the exposures of neighbors, while keeping the index unit's exposure fixed.

The unmeasured confounding is represented by the latent vector \mathbf{U}_{it} . If \mathbf{U}_{it} were observed, the following assumptions would suffice to nonparametrically identify the causal effects:

Assumption 2 (Latent positivity). $f_{\mathbf{D}_{\mathcal{N}_{it}} | \mathbf{X}_{it}, \mathbf{S}_i, \mathbf{U}_{it}}(\mathbf{d} | \mathbf{x}, \mathbf{s}, \mathbf{u}) > 0$ for every $(\mathbf{d}, \mathbf{x}, \mathbf{s}, \mathbf{u})$ in the support.

Assumption 3 (Latent unconfoundedness). $Y_{it}(\mathbf{d}_{\mathcal{N}_{it}}) \perp\!\!\!\perp \mathbf{D}_{\mathcal{N}_{it}} | (\mathbf{X}_{it}, \mathbf{S}_i, \mathbf{U}_{it})$ for all $\mathbf{d}_{\mathcal{N}_{it}}$.

Under Assumptions 1–3, the expectation of the potential outcome is

$$\mathbb{E}[Y_{it}(\mathbf{d}_{\mathcal{N}_{it}})] = \mathbb{E}_{\mathbf{X}, \mathbf{S}, \mathbf{U}}[\mathbb{E}[Y_{it} | \mathbf{D}_{\mathcal{N}_{it}} = \mathbf{d}_{\mathcal{N}_{it}}, \mathbf{X}_{it}, \mathbf{S}_i, \mathbf{U}_{it}]],$$

and any average causal contrast such as the PATE between two vectors $\mathbf{d}_{\mathcal{N}_{it}}^{(1)}$ and $\mathbf{d}_{\mathcal{N}_{it}}^{(2)}$ is identified.

Since \mathbf{U}_{it} is unobserved, adjustment is limited to the observed covariates $(\mathbf{X}_{it}, \mathbf{S}_i)$ and causal effects are not identifiable without additional assumptions. In spatial analyses, spatial

smoothness assumptions provides a crucial bridge between observed data and unmeasured confounders. To mitigate confounding bias, a common approach is to model unmeasured confounding as a spatially varying confounder, assuming that its variability is fully captured by spatial location. However, in practice, \mathbf{U} often exhibits both spatial and non-spatial variation, which makes adjustments based solely on \mathbf{X} and \mathbf{S} insufficient for identifying causal effects. We adopt this perspective throughout the paper. The confounding bias represents the discrepancy between the naive estimate under the assumption of no unmeasured confounding (NUC) and the true causal effect. For PATE, it can be expressed as

$$\text{Bias}(\mathbf{d}^{(1)}, \mathbf{d}^{(2)}) = \mathbb{E}_{\mathbf{X}, \mathbf{S}} [\mathbb{E}[Y_{it} \mid \mathbf{D}_{\mathcal{N}_{it}} = \mathbf{d}_{\mathcal{N}_{it}}^{(1)}, \mathbf{X}_{it}, \mathbf{S}_i] - \mathbb{E}[Y_{it} \mid \mathbf{D}_{\mathcal{N}_{it}} = \mathbf{d}_{\mathcal{N}_{it}}^{(2)}, \mathbf{X}_{it}, \mathbf{S}_i]] \\ - \text{PATE}(\mathbf{d}^{(1)}, \mathbf{d}^{(2)}).$$

Next, we introduce our factor confounding model along with the assumptions under which the bias above becomes identifiable.

3 Factor Confounding

In this section, we formalize how assumptions about low-rank confounding, combined with factor models and negative control style assumptions, can help debias causal effect estimates. Throughout, we assume that, given all observables, the effect of unmeasured confounding on both exposures and outcomes is reflected in the residual correlation, which we model as a rank- M matrix plus a diagonal matrix. For this reason, we refer to our approach as the “factor confounding” model, as it accounts for latent confounders using factor models for both the residual exposures and outcomes. Below, in Section 3.1, we start by outlining the core modeling assumptions of the factor confounding model used to account for residual spatial correlation. We provide identification results in Section 3.2 and in Section 3.3, we briefly discuss tradeoffs between modeling residual spatial vs residual temporal correlation. Finally, we describe our estimation strategy in Section 3.4.

3.1 Model Specification

Here, we present our factor confounding model which accounts for the effect of unmeasured confounders on residual spatial variation, treating time points as independent replicates. Later, we discuss the potential for models which account for the effect of unmeasured confounders on residual temporal correlation.

Assumption 4 (Factor confounding). *Conditional on $(\mathbf{X}_{it}, \mathbf{S}_i)$, both \mathbf{D}_t and \mathbf{Y}_t are linear functions of an unmeasured $\mathbf{U}_t \in \mathbb{R}^M$:*

$$\mathbf{D}_t = f(\mathbf{X}_t, \mathbf{S}) + B\mathbf{U}_t + \boldsymbol{\xi}_t, \quad (1)$$

$$\mathbf{Y}_t = g(\mathbf{D}_t, \mathbf{X}_t, \mathbf{S}) + \Gamma\Sigma_{U|D}^{-1/2}\mathbf{U}_t + \boldsymbol{\varepsilon}_t, \quad (2)$$

where we denote $\mu_{U|D} := \mathbb{E}[\mathbf{U}_t \mid \mathbf{D}_t, \mathbf{X}_t, \mathbf{S}]$ and $\Sigma_{U|D} := \text{Cov}(\mathbf{U}_t \mid \mathbf{D}_t, \mathbf{X}_t, \mathbf{S})$. Marginally, \mathbf{U}_t are i.i.d. mean-zero M -vectors. $\boldsymbol{\xi}_t$ and $\boldsymbol{\varepsilon}_t$ are independent mean-zero random vectors with diagonal covariance Λ_D and Λ_Y respectively. We assume that \mathbf{D}_t does not affect future confounders, so that there is no treatment-confounder feedback (Hernán and Robins, 2020).

Under this model, $\text{Cov}(\text{vec}(\mathbf{D}) \mid \mathbf{X}, \mathbf{S}) = I_T \otimes (BB^\top + \Lambda_D)$ and $\text{Cov}(\text{vec}(\mathbf{Y}) \mid \mathbf{D}, \mathbf{X}, \mathbf{S}) = I_T \otimes (\Gamma\Gamma^\top + \Lambda_Y)$ where $B, \Gamma \in \mathbb{R}^{N \times M}$ are factor loading matrices. Any causal estimand can be written as a function of $g(\mathbf{D}_t) := (g_1(\mathbf{D}_t), \dots, g_N(\mathbf{D}_t))^\top$.

To streamline notation moving forward, we suppress explicit conditioning on the observed covariates and spatial locations, (\mathbf{X}, \mathbf{S}) , but all results hold conditionally on them. The bias arises from the naive regression of \mathbf{Y}_t on \mathbf{D}_t is given by the following proposition.

Proposition 1 (Bias of naive regression). *Under model (2), the naive regression of the outcome vector \mathbf{Y}_t on the exposure vector \mathbf{D}_t gives the conditional moments*

$$\mathbb{E}[\mathbf{Y}_t \mid \mathbf{D}_t] = g(\mathbf{D}_t) + \Gamma\Sigma_{U|D}^{-1/2}\mu_{U|D}, \quad (3)$$

$$\text{Cov}(\mathbf{Y}_t \mid \mathbf{D}_t) = \Gamma\Gamma^\top + \Lambda_Y. \quad (4)$$

Consequently, the naive estimator of g is additively biased by $\text{Bias}(\mathbf{d}) = \Gamma\Sigma_{U|D}^{-1/2}\mu_{U|D}$.

This proposition highlights the parametric link between the outcome mean and covariance. Under this model, exact recovery of g is only possible if the bias term is zero, or under additional assumptions on the magnitude or structure of the causal effects.

To complete the model specification, we need to specify a latent variable model for the exposures that leads to potentially identifiable expressions for $\mu_{U|D}$ and $\Sigma_{U|D}$. While many choices are possible, we focus here on the Gaussian probabilistic PCA formulation (Tipping and Bishop, 1999).

Assumption 5 (Probabilistic PCA exposure model). *Exposures are linear in Gaussian unmeasured confounders with additive Gaussian noise:*

$$\mathbf{D}_t = B\mathbf{U}_t + \boldsymbol{\xi}_t, \quad (5)$$

$$\mathbf{U}_t \sim \mathcal{N}_M(0, I_M), \quad (6)$$

$$\boldsymbol{\xi}_t \sim \mathcal{N}_N(0, \Lambda_D), \quad (7)$$

where Λ_D is a diagonal covariance matrix.

Under this specification, the exposure distribution is $\mathbf{D}_t \sim \mathcal{N}_N(0, \Sigma_D)$ with $\Sigma_D = BB^\top + \Lambda_D$. The joint normality gives $\mathbf{U}_t \mid \mathbf{D}_t \sim \mathcal{N}_M(\mu_{U|D}, \Sigma_{U|D})$, where $\mu_{U|D} = B^\top\Sigma_D^{-1}\mathbf{D}_t$ and $\Sigma_{U|D} = I_M - B^\top\Sigma_D^{-1}B$. Although the normality assumption is strong, we show via simulation that our method is robust even when the outcomes and exposures are non-Gaussian (Appendix Figure 7). This is because our approach ultimately rests on the fact that unmeasured confounders are linear in the exposures. This holds exactly under the probabilistic PCA model but approximately holds in a much wider class of models. Based on this observation, there are several possible approaches for relaxing Assumption 5, but we do not explore them further here (see e.g. Zheng et al., 2024, 2025)

Finally, we note that our method is closely related to the interactive fixed effects (IFE) estimator proposed by Bai (2009), which extends traditional fixed effects models by introducing low-rank time-unit interactions to capture unobserved heterogeneity. Like our approach, the IFE model uses factor structure in both exposures and outcomes to account for heterogeneity and to de-bias estimates of exposure effects. However, there are crucial differences

in both motivation and structure. First, [Bai \(2009\)](#) focus on parameter identification in an asymptotic framework, and do not explicitly address causal identifiability or omitted variable bias, nor do they account for the role of potential interference. Second, they treat all parameters as fixed effects, whereas we consider the implications of a model where shared confounders are random effects that can be marginalized out. This leads to significant performance gains over IFE when either N or T is small, as we show via simulations. Moreover, the IFE model requires outcomes to be linear in the exposures, while our approach can accommodate both nonlinear exposure effects and treatment effect heterogeneity across units. Below, we show how our formulation leads to explicit (partial) identification of causal parameters without relying on asymptotic arguments. We then highlight advantages of our model through simulations in Section 4 and the application in Section 5.

3.2 Identification under Factor Confounding

To bound causal effects even in the presence of unrestricted interference, we must at minimum be able to identify the factor loadings in both the exposure model and the outcome model. The following standard assumption guarantees identifiability of the factor loadings up to rotation.

Assumption 6 (Factor model identifiability). *The outcomes follow Equation (2) and the exposures satisfy (5)-(7). Further, the factor loading matrices B and Γ are of rank M , and for each matrix, removing any row results in two disjoint submatrices, each of full rank M . Under this condition, B and Γ are identifiable up to rotations from the right.*

This assumption typically requires $(N - M)^2 - N - M \geq 0$ and each latent confounder affects at least three exposures and outcomes ([Anderson and Rubin, 1956](#)). Under Assumption 6, we obtain bounds on the omitted variable bias.

Proposition 2. *Under model (2) and Assumptions 5 - 6 the causal effect function, $g(\cdot)$, is partially identified. Let $\check{\Gamma}$ and \check{B} be any matrices such that $\check{\Gamma}\check{\Gamma}^\top = \Gamma\Gamma^\top$ and $\check{B}\check{B}^\top = BB^\top$. Let $\check{\gamma}_i$ denote the i th row of $\check{\Gamma}$. Then the omitted variable bias for the causal effect of the exposure vector \mathbf{d} on the outcome at site i is*

$$Bias(\mathbf{d})_i = \check{\gamma}_i \Theta \check{\Sigma}_{U|D}^{-1/2} \check{B}^\top \Sigma_D^{-1} \mathbf{d} \in \pm \|\check{\gamma}_i\|_2 \|\check{\Sigma}_{U|D}^{-1/2} \check{B}^\top \Sigma_D^{-1} \mathbf{d}\|_2 \quad (8)$$

where $\Theta \in \mathcal{O}_M$ is an $M \times M$ orthogonal matrix. The interval on the right-hand side of (8) is identifiable for all i . Θ , and hence $g(\cdot)$, are not identifiable without further assumptions.

Proposition 2 shows that causal effects are only partially identified under the factor confounding assumption. Additional structural or spatial assumptions are needed to point identify the effects. In this work, we focus on situations with limited neighborhood interference. Specifically, we assume each outcome Y_{it} depends only on exposures within a given neighborhood, that is $g_i(\mathbf{D}_t) = g_i((D_{jt})_{j \in \mathcal{N}_i})$. Under this assumption, exposures at locations $j \notin \mathcal{N}_i$ act as negative controls for Y_{it} , that is, $\frac{\partial g_i(\mathbf{D}_t)}{\partial D_{jt}} = 0$ for all \mathbf{D}_t . In the special case where there is no interference, each outcome Y_{it} depends only on its own local exposure D_{it} , i.e. $g_i(\mathbf{D}_t) = g_i(D_{it})$. Next, we introduce a formal assumption that enables identification of causal effects, even under neighborhood interference.

Assumption 7 (Off-neighborhood rank). *Let γ_i^\top denote row i of Γ and r_j denote column j of matrix $R := \Sigma_{U|D}^{-1/2} B^\top \Sigma_D^{-1} \in \mathbb{R}^{M \times N}$. For each unit i , define its interference neighborhood $\mathcal{N}_i \subseteq \mathcal{I}$ as the set of spatial locations j satisfying $\frac{\partial g_i(\mathbf{D}_t)}{\partial D_{jt}} \neq 0$ for all \mathbf{D}_t . Then, there exist M distinct indices $I_\star := \{i_1, \dots, i_M\} \subseteq \mathcal{I}$ such that*

1. $\{\gamma_{i_\ell}\}_{\ell=1}^M$ form a basis of \mathbb{R}^M ;
2. for each $\ell = 1, \dots, M$, the submatrix $R_{J(i_\ell)} := (r_j)_{j \notin \mathcal{N}_{i_\ell}} \in \mathbb{R}^{M \times (N - |\mathcal{N}_{i_\ell}|)}$ has full row rank M .

Intuitively, this assumption guarantees that at least M units have enough exposures outside their own interference neighborhoods to span all M latent confounding directions. In many applications, the number of latent confounders M and the size of each neighborhood $|\mathcal{N}_i|$ are both much smaller than the number of spatial units N , so Assumption 7 will hold. This assumption leads to the following identification result.

Theorem 1. *Under model (2) and Assumptions 5 - 7, the causal effect functions, $g_i((D_{jt})_{j \in \mathcal{N}_i})$, are identified for all i .*

We briefly provide intuition for this result. Define the rank- M bias matrix as $C := \Gamma \Sigma_{U|D}^{-1/2} B^\top \Sigma_D^{-1}$. Then we have conditional expectation $\mathbb{E}[Y_{it} \mid \mathbf{D}_t] = g_i((D_{jt})_{j \in \mathcal{N}_i}) + (C\mathbf{D}_t)_i$. For any $j \notin \mathcal{N}_i$, any observed association between Y_{it} and D_{jt} given all other exposures must be due to shared confounding, which then point identifies C_{ij} . Assumption 7 ensures that enough entries of C are identified to recover the full bias matrix and thus to identify all causal effects.

3.3 Modeling Spatial versus Temporal Correlation

So far, we have presented a model for residual spatial correlation in which we have replication in time. While this is typical in panel data settings, in some cases, where the residual spatial correlation is expected to be small (e.g. data with high resolution spatial sampling, as in the example in Section 5), it may make more sense to apply our model to account for temporal correlation and treating spatial units as conditionally independent. When modeling temporal correlation, all the results from the previous sections hold, but instead we have $\text{Cov}(\text{vec}(\mathbf{D}) \mid \mathbf{X}, \mathbf{S}) = (BB^\top + \Lambda_D) \otimes I_N$ and $\text{Cov}(\text{vec}(\mathbf{Y}) \mid \mathbf{D}, \mathbf{X}, \mathbf{S}) = (\Gamma\Gamma^\top + \Lambda_Y) \otimes I_N$, where B and Γ are $T \times M$ factor loading matrices.

In practice, we must choose whether to model residual spatial correlation and exploit replication in time, or instead model residual temporal correlation by leveraging replication over spatial units. Somewhat surprisingly, we find that empirically, point estimates of causal effects are not particularly sensitive to whether dependence is modeled across space or across time. Finally, we note that our method can, in principle, be extended to models that account for low-rank residual correlations in both space and time. We leave this for future exploration, as covariance estimation and model selection are nontrivial in more general matrix normal models (see e.g. Hoff, 2016; Efron, 2009).

3.4 Estimation

In this work we primarily focus on a fully Bayesian model for $(\mathbf{D}, \mathbf{Y}) \mid (\mathbf{X}, \mathbf{S})$, which can be implemented using a probabilistic programming language such as Stan (Stan Development Team, 2023). Prior distributions are placed on all model parameters, including the factor loading matrices B and Γ . The likelihood is specified according to an outcome model based on the moments (3)-(4) and the probabilistic PCA exposure model (5) - (7). Inference via MCMC (or variational Bayes) leads to posterior distributions for all parameters, including the causal estimands of interest. By Theorem 1, these effects are identifiable given sufficient assumptions on the factor structure and interference pattern (Assumptions 5 - 7). Even when the causal effects are not fully identified, posterior distributions will reflect appropriate uncertainty within the partial identification region implied by Proposition 2. This method is applied in the simulation studies (Section 4) and in the PM_{2.5}-birthweight analysis (Section 5).

When estimating linear causal effects, we can reduce bias by first orthogonalizing the exposure and the outcome with respect to observed covariates using double machine learning (DML; Chernozhukov et al., 2018) and then fitting the low-rank factor model to the residuals. Nonlinear or heterogeneous effects can be accommodated either through a precomputed basis expansion or within a fully probabilistic framework. In our application, we adopt a separable specification: the exposure is standardized and a centered cubic B-spline basis is constructed outside the sampler. The outcome mean then combines a linear term in the exposure with spline-based nonlinear components, preprocessed covariates, and the bias term, while the exposure and outcome covariances are jointly modeled through the latent factor structure. For continuous exposures, we summarize posterior draws by reporting the centered dose-response curve $g(d) - g(\bar{d})$ with pointwise credible bands, the marginal effect $g'(d) = \partial g(d) / \partial d$, the average causal derivative ACD = $\mathbb{E}[g'(D)]$, and the average treatment effect of a shift, ATE(Δ) = $\mathbb{E}[g(D + \Delta) - g(D)]$. These quantities are computed from analytic derivatives and spline differences over the empirical exposure distribution.

Finally, as an alternative to the fully Bayesian approach, we also propose a non-Bayesian three-step estimator that may be more suitable for handling high-dimensional data or when more complicated nonlinear functional forms are required. Details of the algorithm and rank selection are provided in Appendix B.

4 Simulation Study

In this section, we assess the performance of our proposed factor confounding model in a number of simulated examples. We begin in Section 4.1 by comparing the estimation error across several benchmark methods. In Section 4.2, we examine the robustness of the method under model misspecification.

4.1 Comparison of Estimators

We compare the performance of our factor confounding approach to a number of alternative estimators under data generated from the proposed model (2), (5)-(7) with $N = 50$ locations, $T = 100$ time points, and $M = 3$ unmeasured confounders. For simplicity, we assume the

causal effect is homogeneous and linear with $g_i(\mathbf{D}_t) = D_{it}$. We also assume no interference across locations, while allowing both exposures and outcomes to contain spatiotemporal components.

We compare seven estimators. The first three are baseline approaches that treat unmeasured confounding as a smooth function of location (and time) following [Gilbert et al. \(2021\)](#), and apply DML either (i) separately at each time point (“Single DML”), (ii) jointly across all locations (“Multi DML”), or (iii) on the entire stacked NT observations (“Stacked DML”). We then consider four additional estimators that incorporate factor modeling procedure to account for unmeasured confounding: (iv) a pure M -factor model fitted jointly to (\mathbf{D}, \mathbf{Y}) (“FC(M)”); (v) a hybrid approach that first partials out spatiotemporal variation with DML before fitting the M -factor model (“FC(M)+DML”); (vi) the IFE estimator with M latent factors (“IFE(M)”); and (vii) an IFE variant applied to DML residuals (“IFE(M)+DML”).

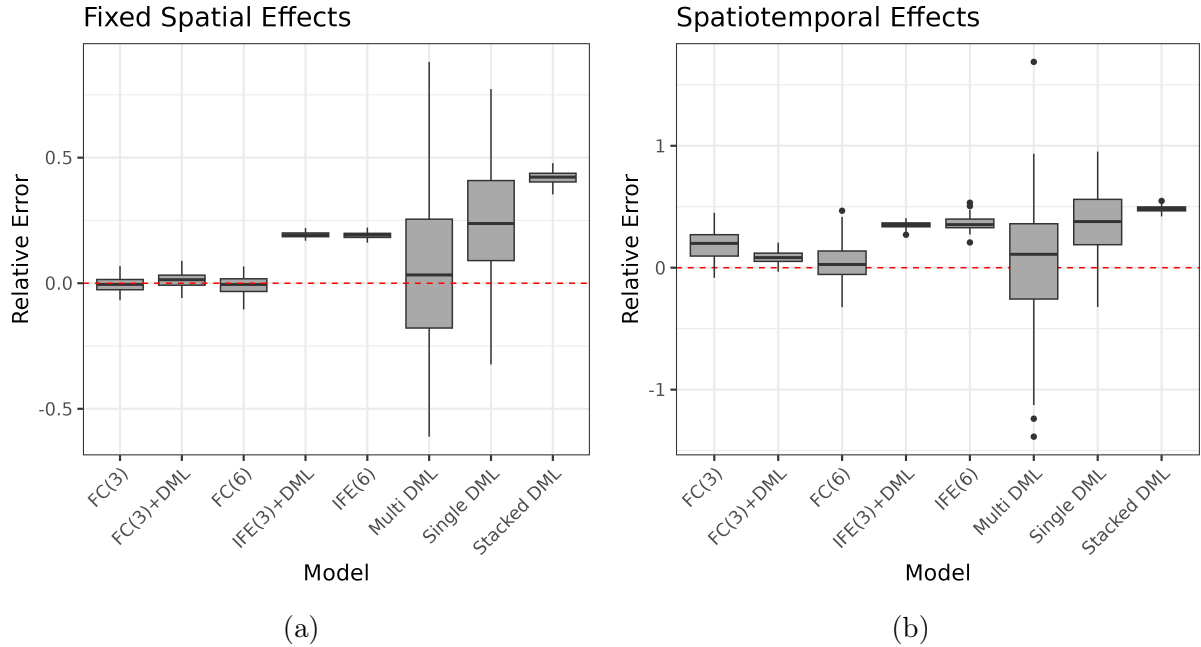


Figure 1: Relative error of estimated causal effects under (a) fixed spatial effects and (b) spatiotemporal effects.

Figure 1 depicts box plots of the estimates from each of these methods across 100 simulated datasets. The naive DML variants are biased because they fail to account for the effect of unmeasured confounders on residual heterogeneity. The IFE estimator is suboptimal when unmeasured confounding dominates the idiosyncratic noise, or when either N or T is small (see Appendix C.2 for a more detailed comparison). In contrast, the hybrid factor confounding approach and the pure factor model with a sufficient number of latent factors appear to yield the most accurate causal effect estimates.

Several additional simulation settings and results are provided in Appendix C. We first examine a scenario with spatial neighborhood interference, where the outcome at each location is influenced not only by the local exposure but also by the exposures of nearest spatial neighbors. Again, only the factor confounding models are unbiased for both direct and

neighborhood effects. We also include an illustrative example with heterogeneous, nonlinear effects. In this setting, we recover unbiased causal effects which vary across spatial units and exhibit nonlinear dependence on the exposure.

4.2 Factor Confounding Under Model Misspecification

Next, we evaluate the robustness of our method to violations of the normality assumption. A key assumption in our framework is that the mean of the unmeasured confounders is linear in the exposure, which is guaranteed when exposures and unmeasured confounders are jointly Gaussian. As such, we explore the performance of our method when the unmeasured confounders and residual errors are non-Gaussian. Specifically, we consider Laplace, t -, mixture-of-normal, and skewed normal distributions. We also investigate a setting with heteroskedastic residuals in both the outcomes and exposures. As shown in Appendix Figure 7, none of the results for any method appear to be sensitive to the data generating assumptions. Notably, the factor confounding estimator remains essentially unbiased across all scenarios, in contrast to alternative approaches. Thus, although Assumption 5 underpins the theoretical results for the factor confounding approach, it appears to be highly robust to departures from Gaussianity.

5 The Causal Effect of $PM_{2.5}$ on Birth Weight

Birth weight is a crucial determinant of infant health and long-term socioeconomic and health outcomes, with low birth weight recognized as a significant risk factor for higher mortality and developmental complications. A recent umbrella review on air pollution and birth outcomes finds a negative association between exposure to $PM_{2.5}$ and birth weight (Nyadanu et al., 2022), reinforcing the growing body of evidence linking prenatal $PM_{2.5}$ exposure to reduced birth weight. However, causal effect estimates vary across studies due to differences in population, exposure measurement, and the analytical approach. For instance, a meta-analysis by Gong et al. (2022) estimated that a $10 \mu g/m^3$ increase in $PM_{2.5}$ exposure during pregnancy leads to an average birth weight reduction of $17 g$ (95% CI: $[-20, -13]$), with high between-study heterogeneity (range from $-79 g$ to $25 g$). Other meta-analyses (Ghosh et al., 2021; Uwak et al., 2021) reported greater reductions of $22 g$ (95% CI: $[-32, -12]$) and $28 g$ (95% CI: $[-48, -7]$) for the same exposure increment. Gilbert et al. (2021) estimate a $-16 g$ (95% CI: $[-28, -3]$) reduction using a nonlinear heterogeneous DML estimator assuming unmeasured confounding is a measurable function of the spatial location. These modest discrepancies highlight the challenges posed by confounding and measurement variability in existing research, underscoring the need for robust causal inference methods to more accurately quantify the impact of prenatal $PM_{2.5}$ exposure on birth outcomes.

In this study, we analyze ZIP code-level birth weight data spanning from 2018 to 2024, obtained from the California Vital Data (Cal-ViDa) Query Tool (State of California, Department of Public Health, 2025). Annual birth counts are reported in nine weight categories: $500\text{--}999 g$, $1000\text{--}1499 g$, $1500\text{--}1999 g$, $2000\text{--}2499 g$, $2500\text{--}2999 g$, $3000\text{--}3499 g$, $3500\text{--}3999 g$, and $4000\text{--}5999 g$, and unknown. For privacy protection, data are suppressed when fewer than 11 births are recorded in a given category. To approximate the full data, we impute these

values using a quasi-Poisson model fitted to the non-missing data, followed by normalization to match the reported total births within each ZIP–year stratum. We then approximate the birth weight distribution within each stratum using a normal density and estimate the mean by maximizing the empirical likelihood. Finally, ZIP codes with fewer than 11 total births in any year are excluded from the analysis, resulting in a dataset of 1,209 ZIP codes observed over seven years. The exposure variable, annual ZIP-level $PM_{2.5}$ concentration, is calculated from high-resolution ($0.01^\circ \times 0.01^\circ$) estimates developed by [Shen et al. \(2024\)](#), which integrate information from satellite, simulation, and ground-based monitoring data.

We adjust for a range of potential confounders, including both environmental and socioeconomic variables measured at the ZIP code level. Parental demographic covariates, constructed from stratified birth count data provided by Cal-ViDa, capture the proportions of births by maternal age group, race/ethnicity, education level, country of birth, and trimester of prenatal care initiation. The dataset includes 26 covariates, organized into six groups: (1) maternal age distribution (nine categories, representing the proportion of births to mothers aged 15 years and under through 50 years and over), (2) race/ethnicity composition (seven categories: White, Black/African-American, Native American/Alaskan Native, Asian, Pacific Islander/Native Hawaiian, Hispanic, and Multi-Race), (3) educational attainment (four levels, from no high school diploma to graduate degree completion), (4) nativity (percentage of foreign-born mothers), (5) prenatal care timing (percentage of pregnancies initiating care in each trimester or receiving no prenatal care), and (6) annual median household income obtained from [Manson et al. \(2024\)](#).

These covariates capture important demographic composition and healthcare access patterns across ZIP codes, but may not fully account for all sources of confounding in the relationship between $PM_{2.5}$ and birth weight. Residual confounding may persist due to additional unmeasured factors such as overall maternal health conditions, health-related behaviors, and parity. Regional factors including industrial activity, healthcare accessibility, and environmental conditions (e.g., green space, temperature, humidity), some of which remain stable over the study period, may also contribute to unmeasured confounding.

In this analysis, we start by modeling the causal effect using a variant of generalized additive models that accommodates nonlinear $PM_{2.5}$ effects while adjusting for factor confounding (see Section 3.4). In contrast to the simulations in Section 4, given the high density of spatial locations and small number of yearly observations, we treat ZIP codes as independent observations and apply the factor model to capture residual temporal correlation instead. For the factor model, we fix the number of latent factors at $M = 3$, reflecting two considerations: (i) identification under the factor confounding assumption with seven years of data requires at most rank 3; and (ii) in practice, modestly overestimating the number of latent factors rarely degrades performance.

Figure 2 shows the inferred dose-response function (left) and marginal effect (right) of $PM_{2.5}$ on birth weight after the factor confounding adjustment. We estimate the average treatment effect for a $10 \mu\text{g}/\text{m}^3$ change in $PM_{2.5}$ as $\mathbb{E}_D[g(D + 10) - g(D)] = -14.9 \text{ g}$ with a 95% credible interval of $(-24.3, -5.6)$. The average causal derivative is $\mathbb{E}_D[g'(D)] = -1.4$ with a 95% credible interval of $(-2.3, -0.4)$. Both of these estimates are broadly in agreement with previously published estimates. In general, we find that below the population median $PM_{2.5}$ level of $9.3 \mu\text{g}/\text{m}^3$, there is little evidence that increases in the exposure cause changes in birth weight. However, above the median, a unit increase in $PM_{2.5}$ causes an average

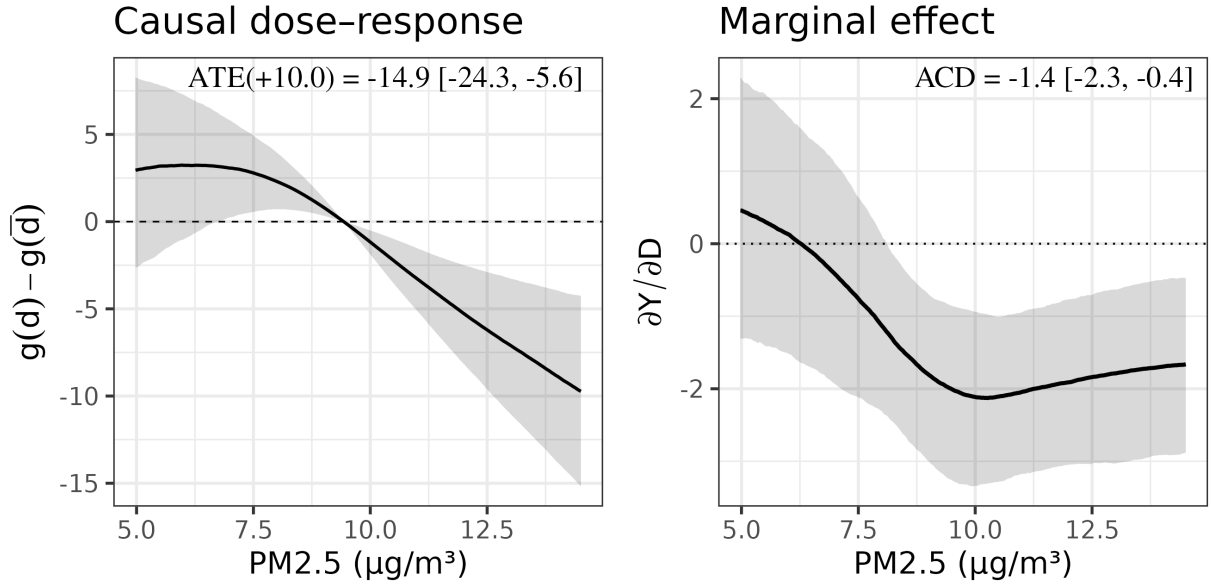


Figure 2: Estimated causal dose-response curve and marginal causal effect under factor confounding. Left) The centered causal dose-response function. On average, a $10 \mu\text{g}/\text{m}^3$ increase in $\text{PM}_{2.5}$ exposure corresponds to a 14.9 g decrease in birth weight. Right) The marginal effect of $\text{PM}_{2.5}$ on birth weight, as a function of exposure. The average causal derivative is about -1.4 . Both plots indicate little evidence of an effect at the lowest exposure levels, but a reduction of about 2 g in birth weight per unit increase in $\text{PM}_{2.5}$ above the median exposure level.

reduction of approximately 2 g .

To demonstrate the robustness of the factor confounding approach on this dataset, we next compare the causal effect estimates when explicitly leaving out potentially important measured confounders (Figure 3). By leaving out different subsets of covariates, we can assess how sensitive each estimator is to the presence of unmeasured confounding. We always adjust for spatial location and year, while varying the exclusion of the six remaining covariate groups. We compare three different estimators: DML under the NUC assumption, the IFE model, and our factor confounding method. For comparability with IFE, the factor confounding adjustment is applied within a partially linear specification in which the outcome is modeled as linear in the exposure. In the left panel of Figure 3, we plot the causal effect estimates, grouped by the number of included covariate groups and colored by the estimator. Unsurprisingly, variation in estimates is greatest when the fewest covariates are included. In contrast, each estimator yields comparable estimates when all covariates are included, presumably because we reduce the residual correlation by conditioning on more potential confounders. The right panel of Figure 3 shows the standard deviation of estimates by estimator and the number of included covariates, as another way to visualize the sensitivity of each estimator to potential unmeasured confounding. DML (NUC), which does not incorporate any adjustment for unmeasured confounding exhibits substantial sensitivity to the adjustment set, exceeding the variability of both factor confounding and IFE estimates

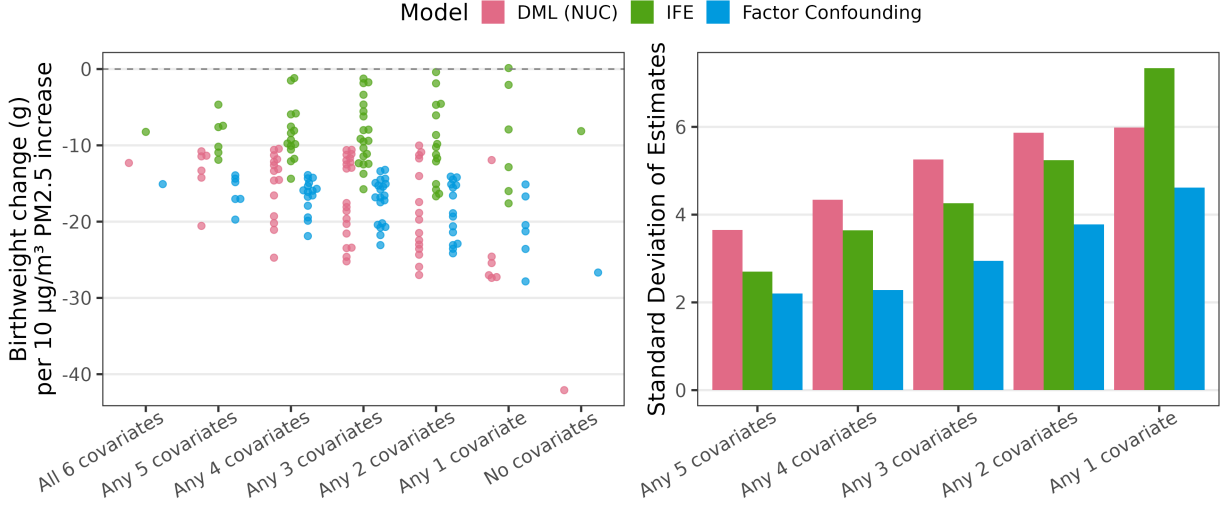


Figure 3: Left) Comparison of effect estimates when controlling for all $\binom{6}{k}$ subsets of confounders, using standard DML, DML combined with the IFE model, and DML combined with factor confounding. Right) Standard deviations of estimates with different number of covariates excluded. In all cases, factor confounding estimator exhibits the least variability under the exclusion of potential confounders, suggesting greater robustness to omitted variables than either IFE or the standard spatial confounding approaches.

in almost all settings. IFE exhibits the second highest variability in estimates in nearly all settings, except when only one covariate group is included, where it shows the greatest variability. In contrast, the factor confounding model consistently yields the most stable estimates, showing the least sensitivity to the choice of included covariates relative to IFE and DML (NUC).

Further, although the true causal effect is unknown, estimates from the factor confounding approach align more closely with previously published results. In Appendix Figure 8, we plot the RMSE of the estimates against the hypothetical causal effect across all $\binom{6}{k}$ covariate subsets, colored by model and faceted by k . Factor confounding consistently achieves the lowest RMSE for nearly all values of k when the true causal effect is about -15 g or smaller, whereas IFE tends to perform better when the effect exceeds -15 g . Prior meta-analyses and causal studies suggest effects in the range of -16 g to -28 g (Ghosh et al., 2021; Gilbert et al., 2021; Uwak et al., 2021; Gong et al., 2022), supporting the plausibility of the factor confounding estimates.

Finally, we examine the potential for interference by considering both the average exposure of the five nearest neighbors and the impact of prior-year pollution. Across DML (NUC), IFE, and factor confounding estimator, the estimated interference effects are all small and not statistically significant (Appendix Figure 9). However, for the direct effect, only the factor confounding estimator yields a stable and statistically significant estimate, whereas DML (NUC) and IFE fail to recover the signal.

6 Discussion

In this work, we introduced a model for spatiotemporal causal inference with unmeasured confounding. We specifically focus on data with continuous exposures and shared unmeasured confounders. To account for bias from such confounders, we propose a model motivated by ideas from the causal panel data and multivariate causal inference literature. In particular, when the outcomes and exposures are linear in the unmeasured confounders, a factor modeling framework can be applied to identify causal effects, even in the presence of treatment effect heterogeneity, nonlinearity, or interference. We show that the causal effects are partially identified under our so-called “factor confounding” assumption, and demonstrate how additional (typically weak) assumptions which limit the amount of neighborhood interference can be used to point identify causal effects.

There are several extensions worth considering. Our theoretical results rest on several assumptions such as linearity in the unmeasured confounders, Gaussianity of residuals, and the absence of treatment–confounder feedback (Hernán and Robins, 2020). We show in simulation that the results are not sensitive to the Gaussianity assumption, but we leave any formal extensions involving non-Gaussian or nonlinear relationships for future work. Methods which incorporate our approach into estimation procedures in the presence of treatment–confounder feedback are also warranted. Indeed, in the birth weight application (Section 5), the observed covariates do not perfectly satisfy the factor confounding assumption, which explains why estimates vary when subsets of confounders are systematically held out. To address such concerns, our approach could be combined with additional sensitivity analyses (e.g. in the spirit of Cinelli and Hazlett, 2020). Developing sensitivity analyses tailored to spatiotemporal causal settings remains an important direction for future research.

References

Anderson, T. W. and H. Rubin (1956). Statistical inference in factor analysis. In *Proceedings of the Third Berkeley Symposium on Mathematical Statistics and Probability, Volume 5: Contributions to Econometrics, Industrial Research, and Psychometry*, Volume 3.5, pp. 111–150. University of California Press.

Arkhangelsky, D. and G. Imbens (2024). Causal models for longitudinal and panel data: A survey. *The Econometrics Journal* 27(3), C1–C61.

Aronow, P. M. and C. Samii (2017). Estimating average causal effects under general interference, with application to a social network experiment. *Annals of Applied Statistics* 11(4), 1912–1947.

Bai, J. (2009). Panel data models with interactive fixed effects. *Econometrica* 77(4), 1229–1279.

Bai, J. and S. Ng (2002). Determining the number of factors in approximate factor models. *Econometrica* 70(1), 191–221.

Ben-Michael, E., A. Feller, and E. A. Stuart (2021). A trial emulation approach for policy evaluations with group-level longitudinal data. *Epidemiology* 32(4), 533–540.

Bind, M.-A. (2019). Causal modeling in environmental health. *Annual review of public health* 40(1), 23–43.

Bobb, J. F., M. F. Cruz, S. J. Mooney, A. Drewnowski, D. Arterburn, and A. J. Cook (2022). Accounting for spatial confounding in epidemiological studies with individual-level exposures: An exposure-penalized spline approach. *Journal of the Royal Statistical Society Series A: Statistics in Society* 185(3), 1271–1293.

Chernozhukov, V., D. Chetverikov, M. Demirer, E. Duflo, C. Hansen, W. Newey, and J. Robins (2018). Double/debiased machine learning for treatment and structural parameters. *The Econometrics Journal* 21(1), C1–C68.

Cinelli, C. and C. Hazlett (2020). Making sense of sensitivity: Extending omitted variable bias. *Journal of the Royal Statistical Society Series B-Statistical Methodology* 82(1), 39–67.

Diez Roux, A. V. (2001). Investigating neighborhood and area effects on health. *American journal of public health* 91(11), 1783–1789.

Dupont, E., S. N. Wood, and N. H. Augustin (2022). Spatial+: a novel approach to spatial confounding. *Biometrics* 78(4), 1279–1290.

Efron, B. (2009). Are a set of microarrays independent of each other? *The annals of applied statistics* 3(3), 922.

Ghosh, R., K. Causey, K. Burkart, S. Wozniak, A. Cohen, and M. Brauer (2021). Ambient and household pm2. 5 pollution and adverse perinatal outcomes: a meta-regression and analysis of attributable global burden for 204 countries and territories. *PLoS medicine* 18(9), e1003718.

Gilbert, B., A. Datta, and E. Ogburn (2021). A causal inference framework for spatial confounding. *arXiv preprint arXiv:2112.14946*.

Gong, C., J. Wang, Z. Bai, D. Q. Rich, and Y. Zhang (2022). Maternal exposure to ambient pm2. 5 and term birth weight: a systematic review and meta-analysis of effect estimates. *Science of The Total Environment* 807, 150744.

Guan, Y., G. L. Page, B. J. Reich, M. Ventrucci, and S. Yang (2023). Spectral adjustment for spatial confounding. *Biometrika* 110(3), 699–719.

Hernán, M. A. and J. M. Robins (2020). *Causal Inference: What If*. Boca Raton: Chapman & Hall/CRC.

Hodges, J. S. and B. J. Reich (2010). Adding spatially-correlated errors can mess up the fixed effect you love. *The American Statistician* 64(4), 325–334.

Hoff, P. D. (2016). Limitations on detecting row covariance in the presence of column covariance. *Journal of Multivariate Analysis* 152, 249–258.

Kang, S., A. Franks, M. Audirac, D. Braun, and J. Antonelli (2025). Partial identification and unmeasured confounding with multiple treatments and multiple outcomes.

Keller, J. P. and A. A. Szpiro (2020). Selecting a scale for spatial confounding adjustment. *Journal of the Royal Statistical Society Series A: Statistics in Society* 183(3), 1121–1143.

Khan, K. and C. Berrett (2023). Re-thinking spatial confounding in spatial linear mixed models. *arXiv preprint arXiv:2301.05743*.

Lumley, T. and L. Sheppard (2000). Assessing seasonal confounding and model selection bias in air pollution epidemiology using positive and negative control analyses. *Environmetrics: The official journal of the International Environmetrics Society* 11(6), 705–717.

Manson, S., J. Schroeder, D. Van Riper, K. Knowles, T. Kugler, F. Roberts, and S. Ruggles (2024). Ipums national historical geographic information system: Version 19.0. Dataset.

Miao, W., W. Hu, E. L. Ogburn, and X.-H. Zhou (2022). Identifying effects of multiple treatments in the presence of unmeasured confounding. *Journal of the American Statistical Association*, 1–15.

Nyadanu, S. D., J. Dunne, G. A. Tessema, B. Mullins, B. Kumi-Boateng, M. L. Bell, B. Duko, and G. Pereira (2022). Prenatal exposure to ambient air pollution and adverse birth outcomes: an umbrella review of 36 systematic reviews and meta-analyses. *Environmental pollution* 306, 119465.

Paciorek, C. J. (2010). The importance of scale for spatial-confounding bias and precision of spatial regression estimators. *Statistical Science* 25(1), 107.

Papadogeorgou, G., C. Choirat, and C. M. Zigler (2019). Adjusting for unmeasured spatial confounding with distance adjusted propensity score matching. *Biostatistics* 20(2), 256–272.

Papadogeorgou, G. and S. Samanta (2023). Spatial causal inference in the presence of unmeasured confounding and interference. *arXiv preprint arXiv:2303.08218*.

Prim, S.-N., Y. Guan, S. Yang, A. G. Rappold, K. L. Hill, W.-L. Tsai, C. Keeler, and B. J. Reich (2025). A spectral confounder adjustment for spatial regression with multiple exposures and outcomes. *arXiv preprint arXiv:2506.09325*.

Reich, B. J., S. Yang, Y. Guan, A. B. Giffin, M. J. Miller, and A. Rappold (2021). A review of spatial causal inference methods for environmental and epidemiological applications. *International Statistical Review* 89(3), 605–634.

Rubin, D. B. (1974). Estimating causal effects of treatments in randomized and nonrandomized studies. *Journal of educational Psychology* 66(5), 688.

Schnell, P. M. and G. Papadogeorgou (2020). Mitigating unobserved spatial confounding when estimating the effect of supermarket access on cardiovascular disease deaths. *The Annals of Applied Statistics* 14(4), 2069–2095.

Shen, S., C. Li, A. Van Donkelaar, N. Jacobs, C. Wang, and R. V. Martin (2024). Enhancing global estimation of fine particulate matter concentrations by including geophysical a priori information in deep learning. *ACS ES&T Air* 1(5), 332–345.

Shi, X., W. Miao, and E. T. Tchetgen (2020). A selective review of negative control methods in epidemiology. *Current epidemiology reports* 7, 190–202.

Stan Development Team (2023). Stan modeling language users guide and reference manual, version 2.32.

State of California, Department of Public Health (2025). California Vital Data (Cal-ViDa), Birth Query. <https://cal-vida.cdph.ca.gov/>. Last modified Feb 1, 2025.

Tchetgen Tchetgen, E. J., A. Ying, Y. Cui, X. Shi, and W. Miao (2024). An introduction to proximal causal inference. *Statistical Science* 39(3), 375–390.

Thaden, H. and T. Kneib (2018). Structural equation models for dealing with spatial confounding. *The American Statistician* 72(3), 239–252.

Tipping, M. E. and C. M. Bishop (1999). Probabilistic principal component analysis. *Journal of the Royal Statistical Society Series B: Statistical Methodology* 61(3), 611–622.

Uwak, I., N. Olson, A. Fuentes, M. Moriarty, J. Pulczinski, J. Lam, X. Xu, B. D. Taylor, S. Taiwo, K. Koehler, et al. (2021). Application of the navigation guide systematic review methodology to evaluate prenatal exposure to particulate matter air pollution and infant birth weight. *Environment international* 148, 106378.

Vehtari, A., A. Gelman, and J. Gabry (2017). Practical bayesian model evaluation using leave-one-out cross-validation and waic. *Statistics and computing* 27, 1413–1432.

Zheng, J., A. D'Amour, and A. Franks (2025). Copula-based sensitivity analysis for multi-treatment causal inference with unobserved confounding. *Journal of Machine Learning Research* 26(36), 1–60.

Zheng, J., A. D'Amour, and A. Franks (2022). Bayesian inference and partial identification in multi-treatment causal inference with unobserved confounding. In *International Conference on Artificial Intelligence and Statistics*, pp. 3608–3626. PMLR.

Zheng, J., J. Wu, A. D'Amour, and A. Franks (2024). Sensitivity to unobserved confounding in studies with factor-structured outcomes. *Journal of the American Statistical Association* 119(547), 2026–2037.

A Proofs

Proof of Theorem 1

Proof of Theorem 1. **Step 1 (Characterization of bias).** Without loss of generality, we assume $\mathbb{E}[\mathbf{D}_t] = 0$. Joint Gaussianity of $(\mathbf{U}_t, \mathbf{D}_t)$ implies

$$\mathbb{E}[\mathbf{U}_t | \mathbf{D}_t] = B^\top \Sigma_D^{-1} \mathbf{D}_t, \quad \Sigma_{U|D} := \text{Cov}(\mathbf{U}_t | \mathbf{D}_t) = I_M - B^\top \Sigma_D^{-1} B \succ 0.$$

Substituting these into Equation (2) gives the conditional mean

$$\mathbb{E}[\mathbf{Y}_t | \mathbf{D}_t] = g(\mathbf{D}_t) + C\mathbf{D}_t,$$

where $C = \Gamma \Sigma_{U|D}^{-1/2} B^\top \Sigma_D^{-1}$ controls the confounding bias.

Since B and Γ are identified up to independent rotations under Assumption 6, for any rotations $\tilde{B} = B\Theta_1$, $\tilde{\Gamma} = \Gamma\Theta_2$, $\Theta_1, \Theta_2 \in \mathcal{O}_M$, the bias can be written as

$$\tilde{C} = \tilde{\Gamma} \tilde{\Sigma}_{U|D}^{-1/2} \tilde{B}^\top \Sigma_D^{-1} = \Gamma \Theta \Sigma_{U|D}^{-1/2} B^\top \Sigma_D^{-1},$$

where $\Theta := \Theta_2 \Theta_1^\top$ is still an orthogonal matrix. Thus we can fix B and Γ , then Θ remains the only degree of freedom in bias. Note that C is invariant if $\Theta_1 = \Theta_2$, so B and Γ are at most identified up to a common rotation from the right.

Step 2 (Off-neighborhood identification of C). Under partial interference, $g_i(\cdot)$ depends on the exposure vector only through its neighborhood \mathcal{N}_i , so C_{ij} is identified from

$$\partial_{d_j} \mathbb{E}[Y_{it} | \mathbf{D}_t = \mathbf{d}] = C_{ij}, \quad \forall i \in \mathcal{I}, j \notin \mathcal{N}_i.$$

To resolve the rotation indeterminacy and identify the full matrix C , it suffices to show that the mapping from Θ to these identified entries of C is injective.

Step 3 (Injectivity w.r.t. rotations). For any $\Theta \in \mathcal{O}_M$, write

$$C(\Theta) = \Gamma \Theta R, \quad C_{ij} = \gamma_i^\top \Theta r_j.$$

Consider two rotation matrices Θ and Θ' . The off-neighborhood identification of C gives $C_{ij}(\Theta) = C_{ij}(\Theta')$, $\forall j \notin \mathcal{N}_i$, hence

$$[\Gamma(\Theta - \Theta')R]_{ij} = \gamma_i^\top (\Theta - \Theta')r_j = \langle \Theta - \Theta', \gamma_i r_j^\top \rangle_F = 0,$$

where $\langle \cdot, \cdot \rangle_F$ is the Frobenius inner product. Define the set of outer products

$$S := \{\gamma_i r_j^\top : j \notin \mathcal{N}_i\} \subset \mathbb{R}^{M \times M}.$$

By Assumption 7, there exists M linearly independent rows of Γ and sufficient rank in off-neighborhood columns of R to generate a basis of $\mathbb{R}^{M \times M}$, which implies $\text{span}(S) = \mathbb{R}^{M \times M}$. Therefore, it follows that $\Theta = \Theta'$ and the mapping $\Theta \mapsto C(\Theta)$ is injective.

Step 4 (Identification of g). For each i , taking the conditional expectation with respect to D_{it} yields

$$\mathbb{E}[Y_{it} - (C\mathbf{D}_t)_i | D_{it}] = g_i(D_{it}),$$

which is identified once C is known. Non-parametric estimation of g_i requires the usual smoothness and support conditions, which are assumed satisfied. All claims are proved. \square

B Additional Details on Estimation

Algorithm 1 outlines the three-step estimator for causal inference under factor confounding. For inference, we augment the procedure with an additional bootstrap step.

Algorithm 1 Three-step estimator under factor confounding

Input: i.i.d. observations $\{(\mathbf{Y}_t, \mathbf{D}_t, \mathbf{X}_t)\}_{t=1}^T$, number of latent factors M , bootstrap replicates B , number of random initializations N_{init} .

Output: bias matrix \widehat{C} , dose-response functions $\{\widehat{g}_i\}_{i=1}^N$, causal estimand(s) $\widehat{\beta}$, and corresponding confidence regions.

Step I: Off-neighborhood entries of C .

For each $i = 1, \dots, N$, fit the partially linear model

$$Y_{it} = m_i(D_{it}, \mathbf{X}_t) + \sum_{j \notin \mathcal{N}_i} \alpha_{ij} D_{jt} + \xi_{it},$$

where $m_i(\cdot)$ is learned nonparametrically. Set $\widehat{C}_{ij} \leftarrow \widehat{\alpha}_{ij}$ for $j \notin \mathcal{N}_i$ and denote the resulting off-neighborhood matrix by \widehat{C}_{off} .

Step II: Neighborhood entries of C via factor analysis.

1. Regress each exposure D_{it} on \mathbf{X}_t , collect residuals $\widetilde{\mathbf{D}}_t$, and fit an M -factor model to obtain loadings \widehat{B} .
2. Regress each outcome Y_{it} on (D_{it}, \mathbf{X}_t) , collect residuals $\widetilde{\mathbf{Y}}_t$, and fit an M -factor model to obtain loadings $\widehat{\Gamma}$.
3. Compute $\widehat{R} = \widehat{\Sigma}_{V|D, X}^{-1/2} \widehat{B}^\top \widehat{\Sigma}_D^{-1}$ and solve the generalized orthogonal Procrustes problem

$$\widehat{\Theta} = \arg \min_{\Theta \in \mathcal{O}_M} \|(\widehat{\Gamma} \Theta \widehat{R})_{\text{off}} - \widehat{C}_{\text{off}}\|_F^2.$$

Repeat the optimization N_{init} times with independent initializations $\widehat{\Theta}_0$ and retain the optimal solution. Construct $\widehat{C} = \widehat{\Gamma} \widehat{\Theta} \widehat{R}$ and overwrite its off-neighborhood with \widehat{C}_{off} .

Step III: Debiasing and estimation of $\{g\}$.

Obtain the debiased outcomes $Y_{it}^\dagger = Y_{it} - \sum_{j=1}^N \widehat{C}_{ij} \widetilde{D}_{jt}$. For each $i = 1, \dots, N$, fit a model $\widehat{g}_i(\cdot)$ of Y_{it}^\dagger on (D_{it}, \mathbf{X}_t) and compute $\widehat{\beta}$.

Step IV: Bootstrap inference.

Draw B bootstrap samples. For each sample $b = 1, \dots, B$, repeat **Steps I-III** to obtain $\{\widehat{C}^{*(b)}, \widehat{g}^{*(b)}, \beta^{*(b)}\}_{b=1}^B$ and form confidence regions.

The number of latent factors can be chosen using one or more of the following tools:

- **Exploratory diagnostics.** A scree plot, eigenvalue ratio test, or parallel analysis highlights the point where additional factors explain only negligible variance.
- **Information criteria.** Classical BIC, AIC or criteria of [Bai and Ng \(2002\)](#) are widely used to balance model fit against complexity.

- **Stability checks.** Inspect how factor loadings and causal effect estimates vary with the rank, retaining the smallest rank at which these quantities stabilize.
- **Bayesian comparison.** Fit candidate Bayesian factor models that satisfy the factor confounding assumption and evaluate them with Pareto-smoothed importance sampling estimate of leave-one-out predictive loss (PSIS-LOO; [Vehtari et al., 2017](#)).

C Additional Simulation Results

C.1 Additional Metrics for Section 4.1

Table 1: Simulation results for linear homogeneous effect under factor confounding.

Setting	Method	Bias	SD	MSE
Fixed spatial effects	Single DML	0.240	0.209	0.100
	Multi DML	0.011	0.386	0.146
	Stacked DML	0.415	0.026	0.173
	FC(3)	-0.005	0.030	0.0009
	FC(6)	-0.012	0.038	0.0016
	FC(3)+DML	0.012	0.031	0.0011
	IFE(6)	0.193	0.014	0.0374
	IFE(3)+DML	0.194	0.013	0.0378
Spatiotemporal effects	Single DML	0.336	0.290	0.195
	Multi DML	0.053	0.515	0.260
	Stacked DML	0.482	0.027	0.233
	FC(3)	0.174	0.131	0.047
	FC(6)	0.032	0.092	0.010
	FC(3)+DML	0.077	0.048	0.008
	IFE(6)	0.362	0.056	0.134
	IFE(3)+DML	0.345	0.023	0.120

C.2 Additional Comparison of Estimators

For further comparison between DML (NUC), IFE and FC, we simulate panel data with latent factor confounding. Exposure and outcome are both driven by a small number of unobserved factors, plus idiosyncratic noise, with a constant causal effect $\beta = 1$. To control confounding severity, we draw the factor loadings that link factors to exposure and outcome from a bivariate normal with correlation ρ , so larger ρ implies stronger alignment between the two loading vectors and hence more severe latent confounding. We fix the number of units at $N = 50$ and the factor dimension at $M = 3$, and vary the panel length $T \in \{10, 50, 200\}$ to probe different N/T regimes. Confounding strength varies over $\rho \in \{0, 0.5, 0.9\}$. Each (ρ, T) configuration is replicated 50 times. All methods are given the correct factor rank in these simulations. For each cell we report the sampling distribution of $\hat{\beta}$ via box plots, faceted by ρ (rows) and T (columns), with a dashed line at $\beta = 1$.

With weak confounding ($\rho = 0$), all estimators concentrate near the truth, and dispersion shrinks as T increases. At moderate confounding ($\rho = 0.5$), the DML (NUC) baseline shows clear bias; IFE improves with longer panels as factor recovery stabilizes; and the joint FC model remains close to β with smaller spread. Under severe confounding ($\rho = 0.9$), DML (NUC) is substantially biased and can dominate the axis scale; IFE moves toward β as T

grows but remains sensitive when T is small; FC is the most robust overall, with medians near β across T and reduced dispersion. These patterns align with the identification logic: when exposure and outcome share strong low-rank structure, explicit factor adjustment is essential, and pooling information from both sides improves recovery of the confounder space, particularly in shorter panels.

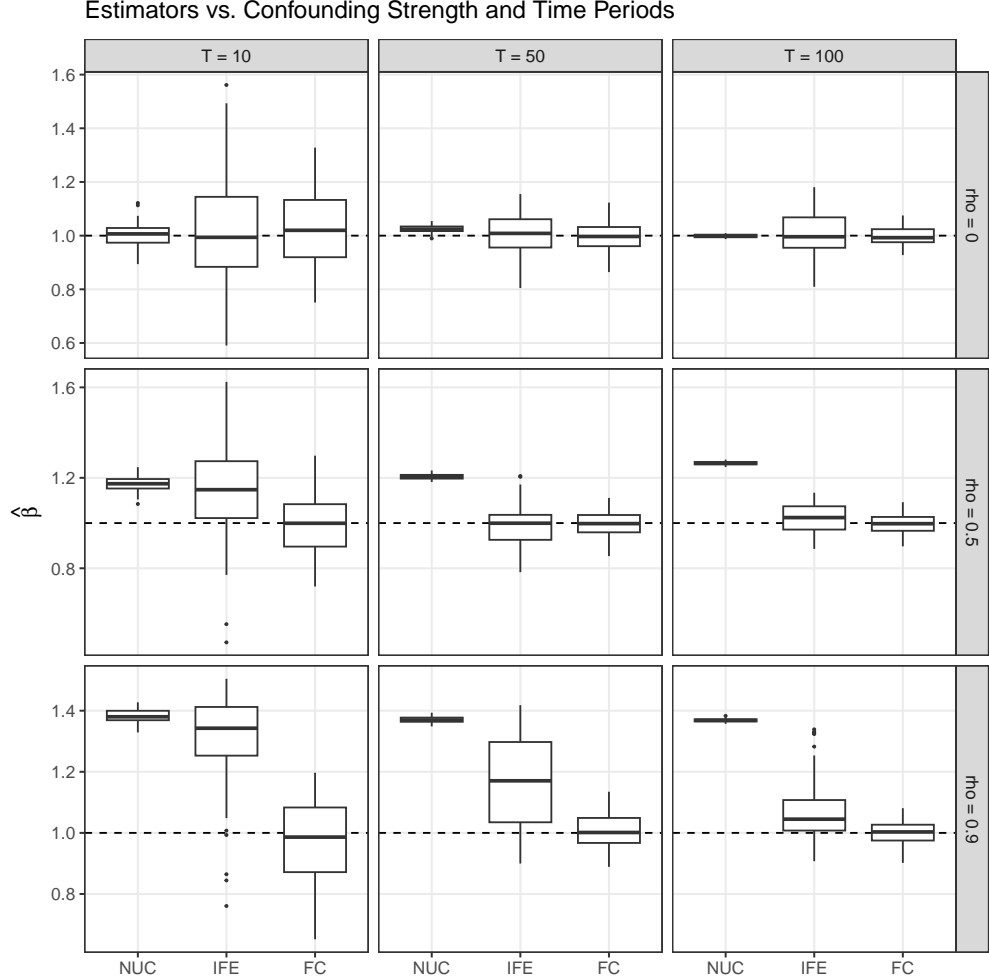


Figure 4: Sampling distributions of $\hat{\beta}$ across replications, faceted by confounding strength ρ (rows) and panel length T (columns). The dashed line marks true effect $\beta = 1$. For readability, we provide facet-specific y -scales.

C.3 Neighborhood Interference

Identification with our approach requires some negative controls but remains applicable in the presence of partial interference. To illustrate this, we examine spatial neighborhood interference, where the outcome at each location is influenced not only by the local exposure but also by the exposures of its three nearest spatial neighbors. We assume the following linear model:

$$Y_{it} = \beta_0 + \beta_1 D_{it} + \beta_2 \bar{D}_{it} + \gamma_i^\top \Sigma_{U|D}^{-1/2} \mathbf{U}_t + \varepsilon_{it} \quad (9)$$

where \bar{D}_{it} denotes the average exposure from the three nearest neighbors, β_1 captures the direct (local) effect, and β_2 describes the indirect (spillover) effect. We generate 100 spatiotemporal datasets under this model, assuming $N = 50$ spatial locations, $T = 200$ time periods, $M = 4$ unmeasured confounders, and true effects $\beta_1 = 1$ and $\beta_2 = 0.5$. Here, we compare three methods for estimation: (i) standard DML without unmeasured confounder adjustment, (ii) the IFE estimator, and (iii) the proposed factor confounding estimator. In Figure 5, we show that both naive DML and IFE are biased in estimating β_1 and β_2 . In contrast, the factor confounding approach provides nearly unbiased estimates of both direct and indirect effects, while also achieving lower variance than IFE.

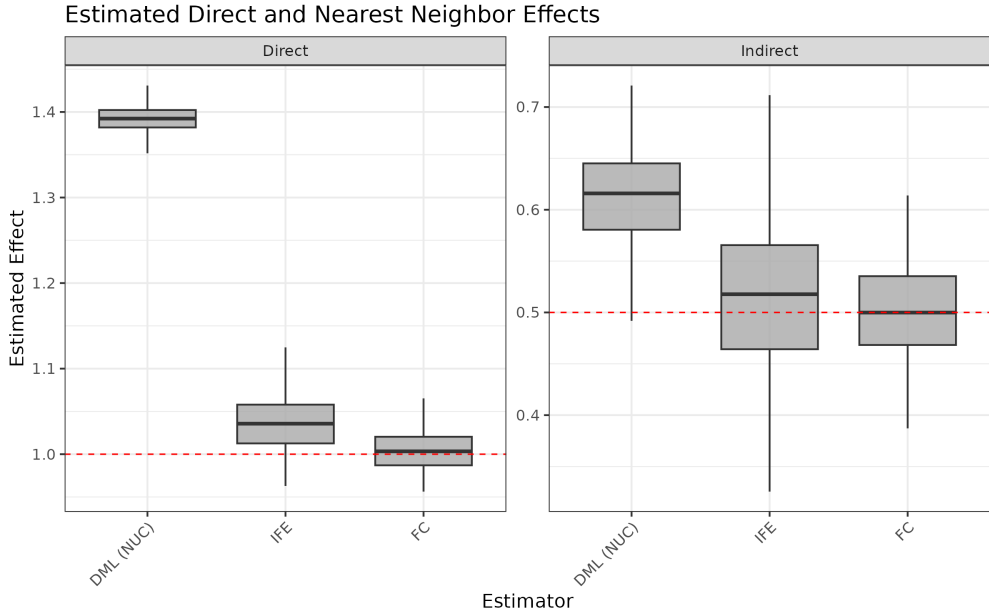


Figure 5: Box plots of causal effect estimates under neighborhood interference across 100 datasets simulated from model (9). Dashed red lines denote the true effects. The factor confounding (FC) estimator outperforms interactive fixed effects (IFE) and standard double machine learning, DML(NUC), yielding lower bias and variance for both direct (β_1) and indirect (β_2) effects.

C.4 Nonlinear Heterogeneous Effects

We consider a simulation for a model with heterogeneous, nonlinear effect and spatially invariant confounding. Set $T = 1000$, $N = 6$, $M = 2$, $p = 2$. The latent and observed variables are: $\mathbf{X}_t \sim \mathcal{N}_p(0, I_p)$, $\mathbf{U}_t \sim \mathcal{N}_M(0, I_M)$, $\boldsymbol{\xi}_t \sim \mathcal{N}_N(0, \sigma_\xi^2 I_N)$, $\boldsymbol{\varepsilon}_t \sim \mathcal{N}_N(0, \sigma_\varepsilon^2 I_N)$, $\sigma_\xi = \sigma_\varepsilon = 0.5$. Parameter matrices are

$$\alpha = \begin{pmatrix} 1.0 & -1.2 \\ 0.8 & 0.5 \\ -0.4 & 1.0 \\ 0.6 & -0.7 \\ 1.5 & 0.9 \end{pmatrix}, \quad B = \begin{pmatrix} 1.0 & 0.3 \\ 0.4 & -0.8 \\ -0.6 & 1.0 \\ -0.7 & -0.3 \\ 1.0 & -0.5 \end{pmatrix}, \quad \tilde{\Gamma} = \begin{pmatrix} 0.4 & -0.7 \\ -0.3 & 0.2 \\ 0.8 & 0.2 \\ 0.2 & 0.7 \\ 0.5 & 0.4 \end{pmatrix}.$$

The exposures and outcomes are generated by

$$D_{it} = \alpha_{i1} \sin X_{1t} + \alpha_{i2} (X_{2t}^2 - 1) + B_i \mathbf{U}_t + \xi_{it},$$

$$Y_{it} = g_i(D_{it}, X_{1t}, X_{2t}) + \tilde{\Gamma}_i \mathbf{U}_t + \varepsilon_{it},$$

where g_i at mean \mathbf{X} is the true effect in Figure 6. As shown in Figure 6, the naive estimates are positively biased for outcomes 1 and 5 and negatively biased for outcomes 2, 3, and 4, whereas our approach successfully removes these biases.

Estimated Dose–Response Functions

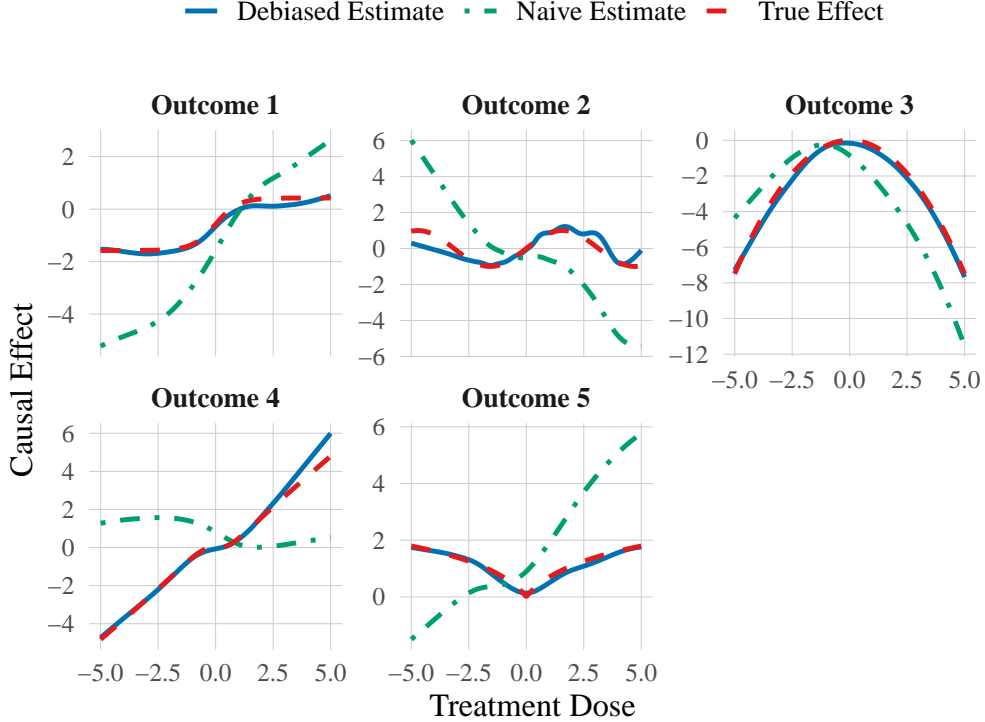


Figure 6: Comparison of estimated and true causal effects for each outcome under the nonlinear setting.

C.5 Figures for Section 4.2

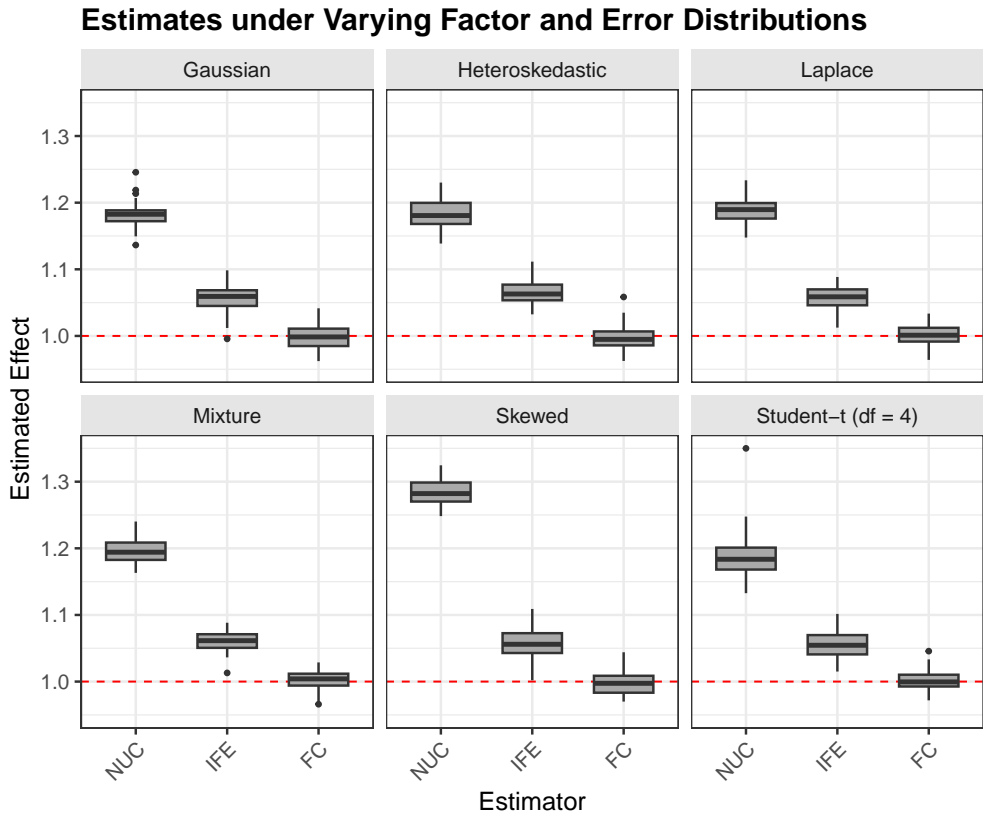


Figure 7: Causal effect estimates under various distributions of unmeasured confounders and residual errors. Dashed red lines denote the true effects.

D Additional Figures for Section 5

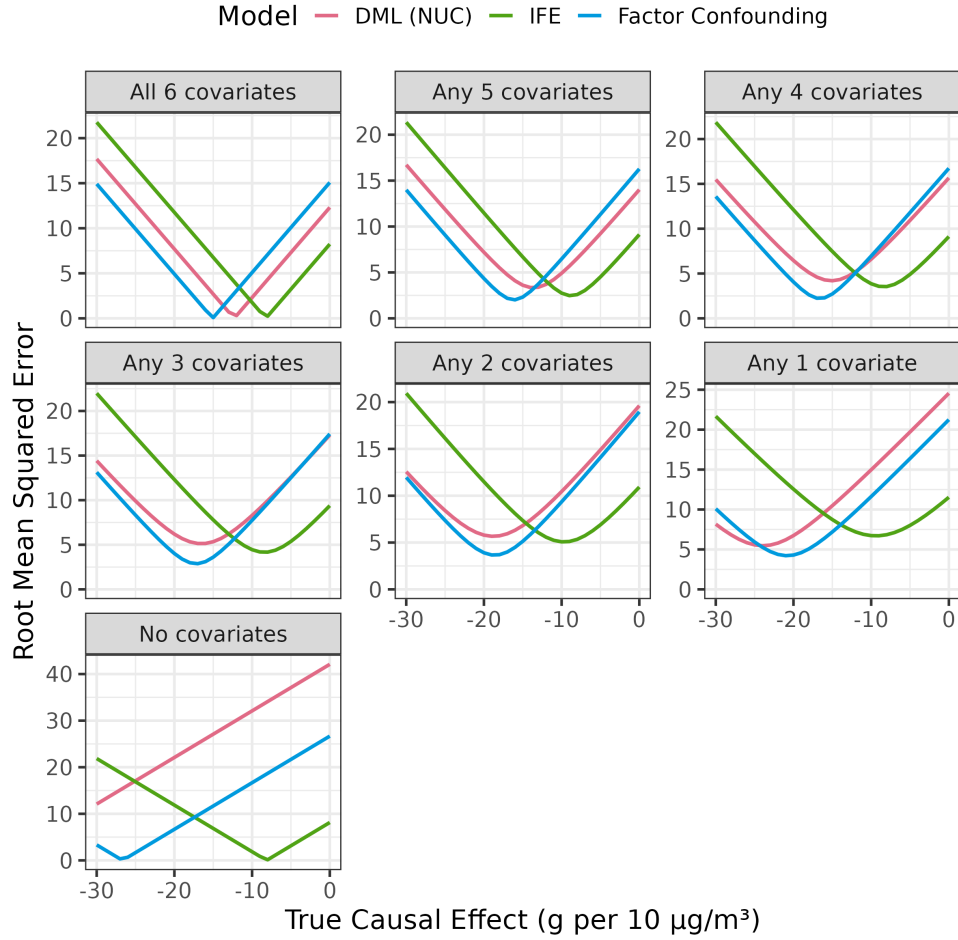


Figure 8: True causal effect versus RMSE of the estimates derived by adjusting for $\binom{6}{k}$ covariate groups, colored by model and faceted by k . Factor confounding (blue) tends to have the lowest RMSE when the true causal effect is less than about -15 g , whereas IFE (green) performs best when the effect is larger than about -12 g . Previous meta-analyses estimate the effect of a $10 \mu\text{g}/\text{m}^3$ increase in $\text{PM}_{2.5}$ on birth weight at around -16 g ([Gong et al., 2022](#); [Gilbert et al., 2021](#)), or even greater reductions in the range of -22 g to -28 g ([Ghosh et al., 2021](#); [Uwak et al., 2021](#)).

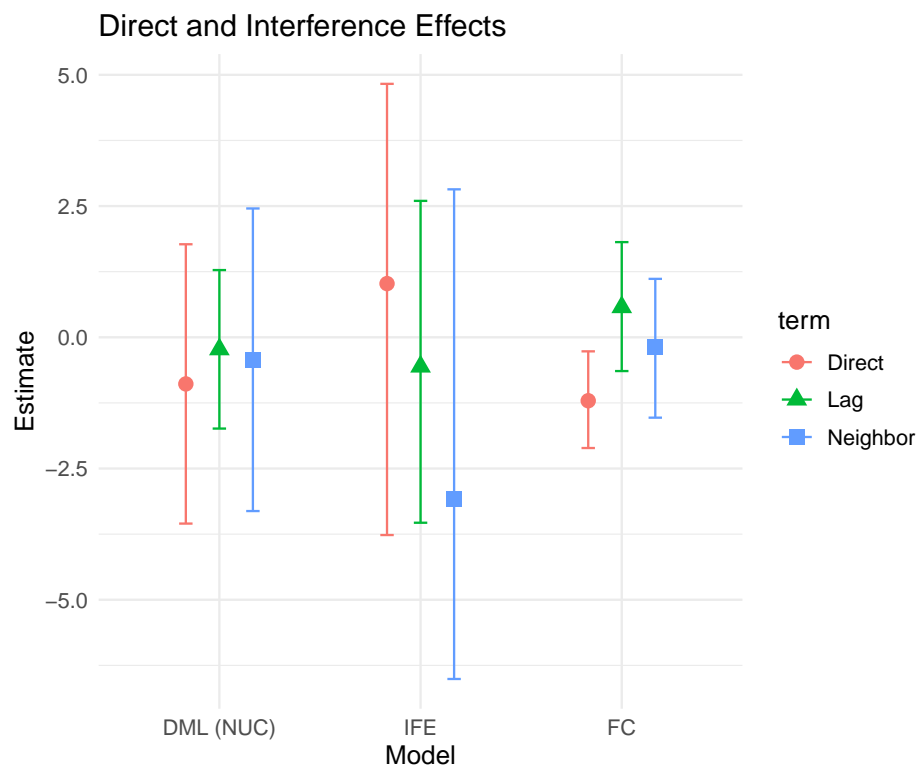


Figure 9: Estimated direct, lag, and neighborhood effects under DML (NUC), IFE, and factor confounding (FC) estimators. The factor confounding method recovers a significant direct effect with greater stability, while interference effects remain weak across all approaches.